International Journal of Metallurgical &
Materials Science and Engineering (IJMMSE)
ISSN(P): 2278-2516; ISSN(E): 2278-2524
Vol. 7, Issue 3, Jun 2017, 1-16

STRUCTURAL, FT-IR AND HOMO-LUMO ENERGY GAP OF 4,4'-DIAMINOOCTAFLUOROBIPHENYL NANO MOLECULAR SWITCH MOLECULE VIA QUANTUM CHEMICAL CALCULATIONS

V. S. LAKSHMEPRIYAA[1], JOE. G. JESUDURAI[2] & K. SELVARAJU[3]

[1,2]*Department of Physics, Loyola college, Chennai, Tamil Nadu, India*

[3]*Department of Physics, Kandaswami Kandar's College, Velur, Namakkal, India*

ABSTRACT

We report a quantum chemical studies of structural, FT-IR, charge density, energy gap and switching behaviour of a single molecular 4,4'-Diaminooctafluorobiphenyl (DAF) molecule. The HF and DFT calculations with B3LYP/6-311G** basis sets were used to determine ground state gas space molecular geometries (bond lengths and bond angles), electron density and bonding features of this molecule. We find that the molecular conformation (switching behavior) varies dramatically DFT method compare with TD-DFT method, which suggests that this system has potential application as a molecular device. The HOMO–LUMO gap calculated from quantum chemical calculations have been compared with the value calculated from the density of states and the values are ~5.021 eV and 4.166 eV for DFT and TDDFT method. The negative electrostatic potential (ESP) is concentrated solely around the F atoms, whereas in the rest of the region a positive ESP to dominate. We hope that the ideas put forward here will facilitate bridging the gap between theory to design a novel molecular-switching materials.

KEYWORDS: DFT, TD-DFT, HOMO-LUMO Energygap, FT-IR & ESP

Received: Feb 20, 2017; **Accepted**: Mar 13, 2017; **Published**: Apr 21, 2017; **Paper Id**.: IJMMSEJUN20171

Original Article

INTRODUCTION

The molecular switches that behave as key units in various optoelectronic devices and smart materials, can specifically switch the physical and chemical properties between two or more states, when stimulating with light, electrochemical or chemical reagents [1,2]. In the past years, the visionary concept of using individual molecules as active electronic components was sketched out by Arieh Aviram and Mark Ratner [3]. In the recent literatures, molecular switches on surfaces have been intensely investigated and research efforts have been devoted to exploring the properties and device opportunities of single molecules [4]. Depending on the properties of the molecules, they can be switched by changing conformations, dipole orientations, spin states, charge states, or even bond formation [5-9]. From such molecules to be used as electronic components, they should be coupled to a support substrate and wired to a molecular circuit without suppressing their switching performance. Further, progress in chemical synthesis has created a broad range of switches and motors, measuring and understanding the physics and chemistry of switching molecules have proved more challenging [10-12]. Fundamental experimental and theoretical studies of a broad range of molecular switches and motors have laid the groundwork for early applications in molecular devices [13].

In general, changes in the physical or chemical properties of the molecular switch are closely related to alterations of the molecular structure. In this sense, those derived from conformational, configurational and/or oxidation-state changes have been need extensively studied [14]. The quantum chemical calculations have been used recently to explain the mechanism of molecular based devices [15]. They are very helpful in understanding the relationship between the confirmation and charge transport properties of a wide range of organic molecular switches [16-17]. The number of theoretical studies on the structural properties of organic compounds is increasing day by day [2]. The polyfluoroaromatic compounds have high optical transparency and thermal stability, in this context 4,4'-Diaminooctafluorobiphenyl molecule is one of the important switch behaviour molecule, because, which is due to the absence of hydrogen atoms and to the fully aromatic molecular structure [18].

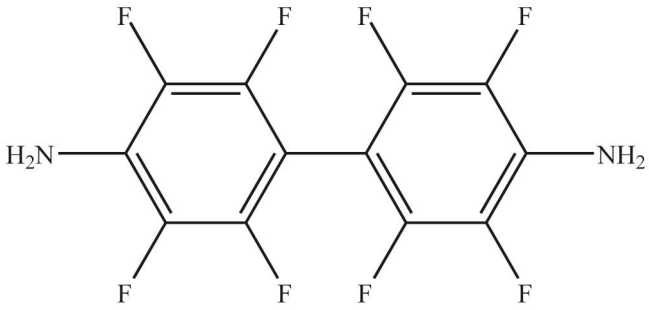

Figure 1: Chemical Structure of 4,4'-Diaminooctafluorobiphenyl (44DF) Molecule

The main objective of this investigation is to calculate the conformational, bond topological properties, such as electron density $\rho(r)$, the Laplacian of electron density $\nabla^2\rho_{bcp}(r)$, the energy density distribution and HOMO-LUMO energy gap and the electrostatic properties of the title compound by DFT method by using B3LYP/6-31G(d,p) level of theory. However, literature survey reveals that to the best of our knowledge, the quantum chemical calculations for 4,4'-Diaminooctafluorobiphenyl have not been reported so far. Therefore, the present investigation using DFT methods of calculations along with theoretical characterization of FT-IR, FT-Raman spectra were undertaken to study the vibrational spectra and various normal modes with greater wave number accuracy. HOMO-LUMO analysis have been carried out to elucidate the information regarding energy gap and charge transfer within the molecule.

COMPUTATIONAL DETAILS

To obtain the exact geometry and the electronic parameters of the 4,4'-Diaminooctafluorobiphenyl (DAF) molecule, a minimum energy structure optimization is carried out from the HF and B3LYP level of theories with the basis sets 6-311G** [19] using Gaussian03 program [20]. All the geometry optimizations were performed via Berny algorithm with the threshold of 0.00045, 0.0003, 0.0018 and 0.0012 au for the maximum force, root mean square force (RMS), maximum displacement and RMS displacement respectively. Here all these quantum chemical calculations were performed for various levels of theories in structural (bond lengths), bond topological (electron density $\rho_{bcp}(r)$, Laplacian of electron density $\nabla^2\rho_{bcp}(r)$ and the electrostatic properties of the molecule, using Bader's theory of "Atoms in Molecules" (AIM), further, the bond topological and the electrostatic properties have been calculated from the EXT94b routine incorporated to the AIMPAC software [21-23]. The Laplacian of the electron density and deformation density maps were plotted using DENPROP and wfn2plots program package [24]. The HOMO–LUMO and electrostatic potential (ESP) maps were plotted using GVIEW [20]. The density of states (DOSs) has been calculated from GaussSum program package [25].

RESULTS AND DISCUSSIONS

Structural Aspects

Figure 2 (a,b) shows the optimized structure of 4,4'-Diaminooctafluorobiphenyl molecule in DFT and TD-DFT methods and, its geometric parameters are presented in Table 1 and 2. This molecules exhibit C_2/C_1 chemical symmetry. The bond distances predicted by HF/6-311G** method are found to be consistently shorter than the DFT/TD-DFT methods (Table 1). The C–C bond lengths calculated from HF method ranged from 1.371 Å to 1.385 Å and the average value is 1.380 Å, interstingly, the calculated C–C bond distances in DFT is almost equal, and its average value is 1.398 Å. Further, the TD-DFT method predicts the C–C distances for the that ranged from 1.386 Å to 1.402 Å and the average value is 1.394 Å, it's found all the C–C bond distance is slightly longer than the distance predicted experimental methods and the difference is 0.0105 Å. The HF and DFT method predicts a bridge bond C(5)–C(7) bond distance is almost equal (~1.480 Å) on compared with the TD-DFT method (1.386 Å). This results reveals that the switching behaviour of 4,4'-Diaminooctafluorobiphenyl molecule. Notably, DFT and TD-DFT methods found slightly longer distances for the C–N (~1.392 Å and ~1.446 Å) bond respectively,, as it was found to be ~0.013 Å lesser when calculated from HF calculations. Notably, the C–F distances (1.341 to 1.352Å) found by DFT are significantly shorter than the HF predicted value (~1.320 Å). The C–H bond distances calculated from all levels of calculations are in the range of 1.083 Å–1.122 Å.

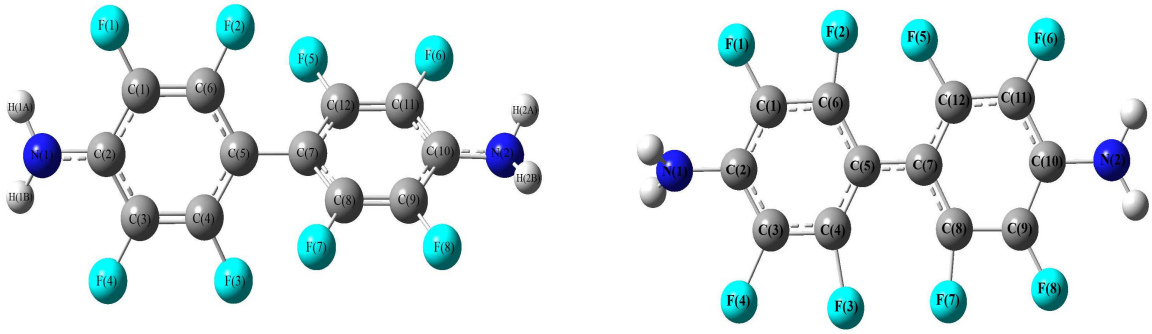

(a) **(b)**

Figure 2: Shows the Optimized Structure of 4,4'-Diaminooctafluorobiphenyl (A) B3LYP (Ground) And (B) TD/DFT

The bond angles C12–C7–C5–C4 and C8–C7–C5–C6 in the centre of C5 atom and their bond angles are ~122.0º for DFT methods and C12–C7–C5–C4 and C8–C7–C5–C6 in the centre of bond angles are ~179.0º respectively. Which confirms that these methods indicating that the switching behaviour of 44DF molecule. So the title compound has good conjugation. The bond angles of C–C–C in benzene ring lies in the range of 115–120º signifying all the carbon atoms are sp_2 hybridized which are in agreement with the literature value.

Table 1

Bond length (Å)	HF	B3LYP(G)	TD-DFT	Exp
C(1)–C(2)	1.385	1.398	1.386	1.384(5)
C(1)–C(6)	1.371	1.383	1.402	1.373(4)
C(2)–C(3)	1.385	1.398	1.386	1.396(4)
C(3)–C(4)	1.371	1.383	1.386	1.376(4)
C(4)–C(5)	1.384	1.398	1.386	1.393(4)
C(5)–C(6)	1.384	1.398	1.400	1.373(4)
C(5)–C(7)	1.484	1.478	1.386	1.478(4)

Table 1: Contd.,				
C(1)–F(1)	1.327	1.352	1.390	1.355(5)
C(3)–F(4)	1.326	1.352	1.563	1.310(4)
C(4)–F(3)	1.314	1.341	1.563	1.355(4)
C(6)–F(2)	1.314	1.341	1.410	1.368(4)
C(2)–N(2)	1.375	1.378	1.446	1.407(4)
C(7)–C(8)	1.384	1.398	1.428	1.384(5)
C(7)–C(12)	1.384	1.398	1.386	1.396(4)
C(8)–C(9)	1.371	1.383	1.476	1.376(4)
C(9)–C(10)	1.385	1.398	1.448	1.393(4)
C(10)–C(11)	1.385	1.398	1.410	1.373(4)
C(11)–C(12)	1.371	1.383	1.412	1.373(4)
C(8)–F(7)	1.314	1.341	1.410	1.355(5)
C(9)–F(8)	1.327	1.352	1.340	1.368(4)
C(11)–F(6)	1.327	1.352	1.320	1.368(4)
C(12)–F(5)	1.314	1.341	1.418	1.355(4)
C(10)–N(1)	1.375	1.378	1.446	1.407(4)

Table 2

Bond Angle (°)	HF	B3LYP	TD-DFT
C(2)–C(1)–C(6)	121.5	121.7	121.0
C(2)–C(1)–F(1)	118.5	118.1	120.0
C(6)–C(1)–F(1)	120.0	120.2	119.0
C(1)–C(2)–C(3)	116.7	116.5	120.0
C(1)–C(2)–N(2)	121.6	121.7	120.0
C(3)–C(2)–N(2)	121.6	121.7	120.0
C(2)–C(3)–C(4)	121.5	121.7	120.0
C(2)–C(3)–F(4)	118.5	118.1	121.5
C(4)–C(3)–F(4)	120.0	120.2	118.5
C(3)–C(4)–C(5)	121.9	121.9	120.0
C(3)–C(4)–F(3)	118.4	118.3	99.7
C(5)–C(4)–F(3)	119.7	119.8	140.3
C(4)–C(5)–C(6)	116.4	116.3	121.1
C(4)–C(5)–C(7)	121.8	121.8	120.0
C(6)–C(5)–C(7)	121.8	121.9	118.9
C(1)–C(6)–C(5)	121.9	121.9	117.9
C(1)–C(6)–F(2)	118.3	118.3	100.2
C(5)–C(6)–F(2)	119.8	119.8	142.0
C(5)–C(7)–C(8)	121.8	121.8	117.4
C(5)–C(7)–C(12)	121.8	121.9	120.0
C(8)–C(7)–C(12)	116.4	116.4	122.6
C(7)–C(8)–C(9)	121.9	121.9	118.6
C(7)–C(8)–F(7)	119.7	119.8	145.9
C(9)–C(8)–F(7)	118.4	118.3	95.5
C(8)–C(9)–C(10)	121.5	121.7	115.0
C(8)–C(9)–F(8)	120.0	120.2	119.6
C(10)–C(9)–F(8)	118.5	118.1	125.3
C(9)–C(10)–C(11)	116.7	116.6	125.5
C(9)–C(10)–N(1)	121.6	121.7	116.2
C(11)–C(10)–N(1)	121.6	121.7	118.2
C(10)–C(11)–C(12)	121.5	121.6	116.6
C(10)–C(11)–F(6)	118.5	118.1	120.1
C(12)–C(11)–F(6)	120.0	120.2	123.4
C(7)–C(12)–C(11)	121.9	121.9	121.7
C(7)–C(12)–F(5)	119.7	119.8	118.3

Table 2: Contd.,			
C(11)–C(12)–F(5)	118.4	118.3	120.0
Torsion Angle (°)			
C(6)–C(1)–C(2)–C(3)	-0.3	-0.5	0.0
C(6)–C(1)–C(2)–N(2)	177.1	176.8	-179.4
F(1)–C(1)–C(2)–C(3)	179.6	179.6	-179.4
F(1)–C(1)–C(2)–N(2)	-2.9	-3.1	1.1
C(2)–C(1)–C(6)–C(5)	0.4	0.6	0.0
C(2)–C(1)–C(6)–F(2)	-179.5	-178.9	-179.4
F(1)–C(1)–C(6)–C(5)	-179.6	-179.5	179.4
F(1)–C(1)–C(6)–F(2)	0.5	1.0	0.0
C(1)–C(2)–C(3)–C(4)	0.0	-0.1	0.0
C(1)–C(2)–C(3)–F(4)	-179.3	-178.9	-179.4
N(2)–C(2)–C(3)–C(4)	-177.5	-177.4	179.4
N(2)–C(2)–C(3)–F(4)	3.3	3.8	0.0
C(2)–C(3)–C(4)–C(5)	0.3	0.6	0.0
C(2)–C(3)–C(4)–F(3)	-179.4	-178.8	-179.4
F(4)–C(3)–C(4)–C(5)	179.6	179.4	179.4
F(4)–C(3)–C(4)–F(3)	-0.1	0.0	0.0
C(3)–C(4)–C(5)–C(6)	-0.3	-0.5	0.0
C(3)–C(4)–C(5)–C(7)	179.8	179.5	179.4
F(3)–C(4)–C(5)–C(6)	179.4	178.8	179.1
F(3)–C(4)–C(5)–C(7)	-0.5	-1.1	-1.5
C(4)–C(5)–C(6)–C(1)	0.0	-0.1	0.0
C(4)–C(5)–C(6)–F(2)	179.9	179.5	179.1
C(7)–C(5)–C(6)–C(1)	179.8	179.9	-179.4
C(7)–C(5)–C(6)–F(2)	-0.3	-0.6	-0.3
C(4)–C(5)–C(7)–C(8)	-63.1	-58.0	0.0
C(4)–C(5)–C(7)–C(12)	117.1	122.1	179.4
C(6)–C(5)–C(7)–C(8)	117.1	122.1	179.4
C(6)–C(5)–C(7)–C(12)	-62.8	-57.9	-1.1
C(5)–C(7)–C(8)–C(9)	179.8	179.5	179.4
C(5)–C(7)–C(8)–F(7)	-0.5	-1.1	0.5
C(12)–C(7)–C(8)–C(9)	-0.3	-0.5	0.0
C(12)–C(7)–C(8)–F(7)	179.4	178.8	-178.9
C(5)–C(7)–C(12)–C(11)	179.8	179.9	-179.4
C(5)–C(7)–C(12)–F(5)	-0.3	-0.6	1.1
C(8)–C(7)–C(12)–C(11)	0.0	-0.1	0.0
C(8)–C(7)–C(12)–F(5)	179.9	179.5	-179.5
C(7)–C(8)–C(9)–C(10)	0.4	0.6	0.0
C(7)–C(8)–C(9)–F(8)	179.6	179.4	-179.4
F(7)–C(8)–C(9)–C(10)	-179.4	-178.8	179.4
F(7)–C(8)–C(9)–F(8)	-0.1	0.0	0.0
C(8)–C(9)–C(10)–C(11)	0.0	-0.1	-0.1
C(8)–C(9)–C(10)–N(1)	-177.5	-177.4	-179.5
F(8)–C(9)–C(10)–C(11)	-179.3	-178.9	179.3
F(8)–C(9)–C(10)–N(1)	3.3	3.8	-0.1
C(9)–C(10)–C(11)–C(12)	-0.3	-0.5	0.1
C(9)–C(10)–C(11)–F(6)	179.6	179.6	-179.3
N(1)–C(10)–C(11)–C(12)	177.1	176.8	179.5
N(1)–C(10)–C(11)–F(6)	-2.9	-3.1	0.1
C(10)–C(11)–C(12)–C(7)	0.4	0.6	0.0
C(10)–C(11)–C(12)–F(5)	-179.6	-178.9	179.5
F(6)–C(11)–C(12)–C(7)	-179.6	-179.5	179.3
F(6)–C(11)–C(12)–F(5)	0.5	1.0	-1.2

ELECTRON DENSITY DISTRIBUTION

Figure 3 (a,b), depicts the deformation density of the molecule calculated from the wave function obtained from DFT and TD-DFT calculation. The deformation density map shows the aspherical nature of the electron density of atoms in molecules, which allows visualizing the areas of charge accumulation in the bonding regions and the lone pair positions of atoms in molecules [26]. The deformation map of 4,4'-Diaminooctafluorobiphenyl molecule reveals the covalent nature of bonds from the continuous region of charge density distribution of the molecule. A complete spectrum of charge density distribution obtained from the bond topological analysis of 4,4'-Diaminooctafluorobiphenyl is presented in Table 3. The electron density $\rho_{bcp}(r)$ at the bcp's of C_{ar}–C_{ar} bonding regions (2.908 $eÅ^{-3}$) are considerably less when compared with the TD-DFT methods and the value is ~1.151 $eÅ^{-3}$. The difference of $\rho_{bcp}(r)$ values among the bonds of the ring, reflect the effect of substituent's (N and F atoms) in the ring. The DFT studies predicted that the high electron density at BCP comes at C–F bonds in both methods found almost equal and the average value is ~1.695 $eÅ^{-3}$for each bond which comes approximately same with the experimentally predicted density. Figure.3 (a,b) shows the lone pair of F-atoms.

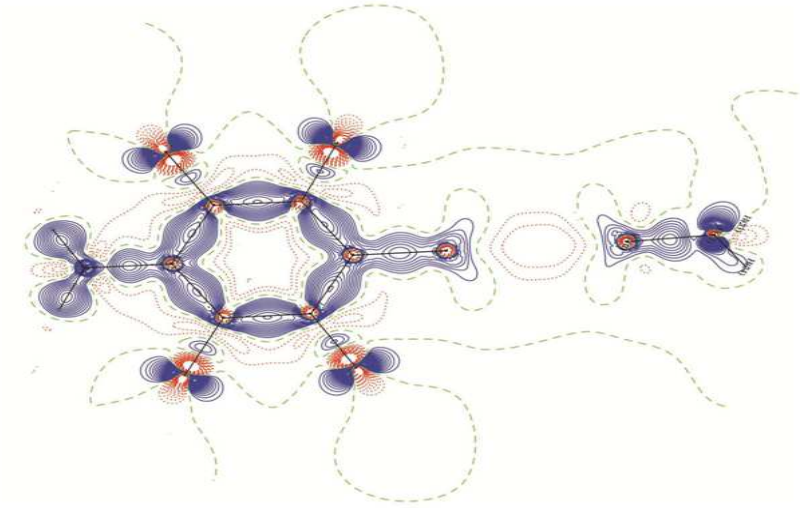

(a)

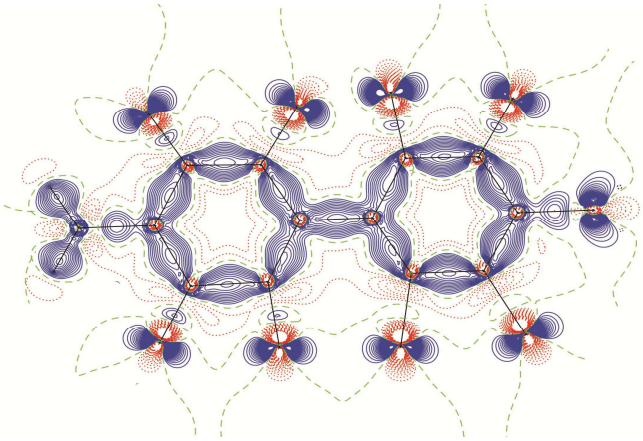

(b)

Figure 3: Theoretical Static Deformation Density Maps (a) DFT and (b) TD-DFT of 44DF Molecules. The Deformation Density Contours Levels were Drawn at ±0.05 $eÅ^{-3}$, Positive Contours are Solid Line, Zero Dashed Line and Negative Contours Dotted Line

The bond ellipticity [27], $\varepsilon = (\lambda_1/\lambda_2\text{-}1)$ is defined as the measure of anisotropy of electron distribution at BCP, where λ_1 and λ_2 are the negative eigen values of Hessian matrix [32]. The high ellipticity value indicates, the large anisotropy of bonding density $\rho_{bcp}(r)$ and hence a strong deviation from π-type bond character [27]. The ellipticity of C–F bonds of DFT and TD-DFT methods are found small and the value ranges 0.04–0.36, indicates, that the bond densities are highly isotropic. Both methods predicted a large ε-values for C(5)–C(7) bonds, shows, the densities are highly anisotropic, and the trend is same in C–N bonds.

Table 3: Bond Topological Properties of 44DF Molecule (First Line Indicates DFT Second Line TD-DFT Level Theory)

Bonds	$\rho_{bcp}(r)^a$	$\nabla^2\rho_{bcp}(r)^b$	ε^c	$\lambda_1{}^d$	$\lambda_2{}^d$	$\lambda_3{}^d$	d_1	d_2	D
C(1)–C(2)	2.098	-20.90	0.31	-16.42	-12.50	8.02	0.704	0.695	1.399
	2.151	-22.05	0.31	-16.99	-12.93	7.87	0.678	0.709	1.387
C(2)–C(3)	2.098	-20.90	0.31	-16.42	-12.50	8.02	0.696	0.704	1.399
	2.137	-21.82	0.31	-16.76	-12.80	7.73	0.718	0.669	1.388
C(5)–C(4)	2.078	-20.33	0.31	-15.94	-12.18	7.79	0.669	0.729	1.398
	2.070	-20.29	0.30	-15.60	-11.99	7.29	0.722	0.666	1.389
C(3)–C(4)	2.172	-22.25	0.41	-17.62	-12.51	7.88	0.691	0.693	1.385
	2.177	-22.37	0.37	-17.56	-12.87	8.06	0.687	0.701	1.388
C(6)–C(5)	2.079	-20.34	0.31	-15.95	-12.18	7.79	0.729	0.669	1.398
	2.017	-19.11	0.30	-15.10	-11.62	7.61	0.677	0.727	1.403
C(5)–C(7)	1.748	-15.00	0.08	-12.07	-11.21	8.28	0.739	0.739	1.478
	2.121	-22.51	0.15	-16.21	-14.15	7.84	0.686	0.700	1.386
C(1)–C(6)	2.171	-22.24	0.41	-17.61	-12.51	7.88	0.691	0.693	1.385
	2.139	-21.56	0.35	-17.23	-12.75	8.43	0.691	0.712	1.403
C(3)–F(4)	1.696	4.01	0.06	-10.99	-10.36	25.37	0.452	0.899	1.352
	1.148	-4.03	0.04	-7.24	-6.98	10.18	0.927	0.637	1.563
F(1)–C(1)	1.695	4.01	0.06	-10.99	-10.35	25.35	0.900	0.452	1.352
	1.600	-2.71	0.04	-10.03	-9.67	16.99	0.476	0.914	1.390
C(9)–F(8)	1.748	4.37	0.04	-11.82	-11.32	27.51	0.893	0.447	1.340
	1.867	-15.74	0.36	-14.38	-10.54	9.19	0.747	0.730	1.477
F(2)–C(6)	1.750	3.73	0.02	-11.81	-11.62	27.16	0.892	0.449	1.341
	1.567	-5.66	0.04	-9.55	-9.40	13.28	0.502	0.909	1.411
N(2)–C(2)	2.091	-22.03	0.12	-15.79	-14.14	7.90	0.842	0.536	1.378
	1.826	-16.73	0.11	-13.35	-12.04	8.66	0.608	0.838	1.446
C(7)–C(8)	2.078	-20.33	0.31	-15.94	-12.18	7.79	0.669	0.729	1.398
	1.904	-16.84	0.30	-13.91	-10.67	7.75	0.752	0.678	1.430
C(8)–C(9)	2.172	-22.25	0.41	-17.62	-12.51	7.88	0.693	0.691	1.385
	1.696	4.02	0.06	-11.00	-10.36	25.38	0.452	0.899	1.352
C(10)–C(9)	2.098	-20.90	0.31	-16.42	-12.50	8.02	0.696	0.704	1.399
	1.902	-16.81	0.31	-14.38	-10.96	8.53	0.720	0.729	1.449
C(12)–C(7)	2.079	-20.34	0.31	-15.95	-12.18	7.79	0.729	0.669	1.398
	2.112	-21.15	0.31	-16.26	-12.43	7.54	0.675	0.712	1.387
C(12)–C(11)	2.171	-22.23	0.41	-17.61	-12.51	7.88	0.693	0.691	1.385
	2.045	-19.45	0.40	-16.24	-11.54	8.33	0.705	0.710	1.415
C(11)–C(10)	2.098	-20.91	0.31	-16.43	-12.50	8.02	0.704	0.695	1.399
	2.047	-19.88	0.30	-15.89	-12.09	8.10	0.706	0.705	1.410
C(10)–N(1)	2.091	-22.03	0.12	-15.79	-14.14	7.90	0.536	0.842	1.378
	1.816	-16.64	0.16	-13.27	-11.49	8.13	0.852	0.594	1.446
F(6)–C(11)	1.696	4.03	0.06	-10.99	-10.36	25.38	0.899	0.452	1.352
	1.820	7.13	0.06	-13.03	-12.32	32.48	0.439	0.881	1.320
F(5)–C(12)	1.750	3.74	0.02	-11.81	-11.62	27.17	0.892	0.449	1.341
	1.538	-6.29	0.03	-9.51	-9.21	12.42	0.503	0.915	1.418
C(8)–F(7)	1.751	3.74	0.02	-11.83	-11.64	27.21	0.449	0.892	1.341

Table 3: Contd.,									
	1.559	-5.53	0.03	-9.53	-9.28	13.28	0.909	0.502	1.411
C(4)–F(3)	1.751	3.73	0.02	-11.83	-11.64	27.20	0.449	0.892	1.341
	1.150	-2.83	0.00	-6.98	-6.95	11.09	0.918	0.648	1.565
N(1)–H(2A)	2.299	-39.27	0.05	-31.08	-29.48	21.29	0.740	0.249	0.988
	2.168	-34.89	0.07	-28.63	-26.86	20.60	0.256	0.753	1.009
H(2B)–N(1)	2.299	-39.28	0.05	-31.08	-29.49	21.29	0.249	0.740	0.988
	2.170	-34.81	0.07	-28.63	-26.85	20.67	0.752	0.257	1.009
H(2B)–N(2)	2.299	-39.27	0.05	-31.07	-29.48	21.29	0.249	0.740	0.988
	2.155	-33.63	0.08	-28.22	-26.18	20.77	0.749	0.260	1.009
H(1A)–N(2)	2.299	-39.26	0.05	-31.07	-29.48	21.29	0.249	0.740	0.988
	2.154	-33.75	0.08	-28.25	-26.23	20.74	0.259	0.750	1.009

[a] Electron density ($eÅ^{-3}$), [b] Laplacian of Electron density ($eÅ^{-5}$), [c]Bond ellipticity, [d]Hessian eigen values ($eÅ^{-5}$), d_1 and d_2 are the distances in Å between CP and respective atoms of the bond in Å.

Frontier of HOMO-LUMO Energy Gap and Electrostatic Potential

The conjugated molecules are characterized by a highest occupied molecular orbital-lowest unoccupied molecular orbital (HOMO–LUMO) separation, which is the result of a significant degree of intermolecular charge transfer (ICT) from the end-capping electron-donor to the efficient electron acceptor group through π-conjugated path [28-30]. The HOMO is the orbital that primarily acts as an electron donor and the LUMO is the orbital that largely acts as the electron acceptor, and the gap between HOMO and LUMO characterizes the molecular chemical stability [30]. The energy gap between the HOMO and the LUMO molecular orbitals is a critical parameter in determining molecular electrical transport properties because it is a measure of electron conductivity The HOMOs are localized mainly on the benzene ring system [30].

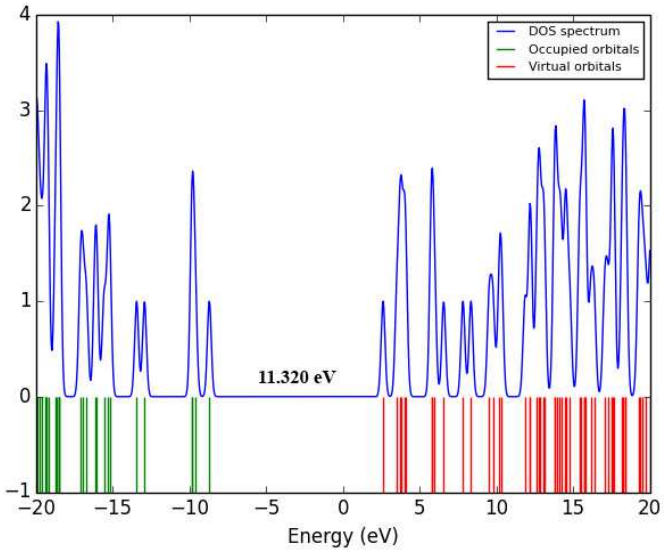

(a) HF/6-311G**

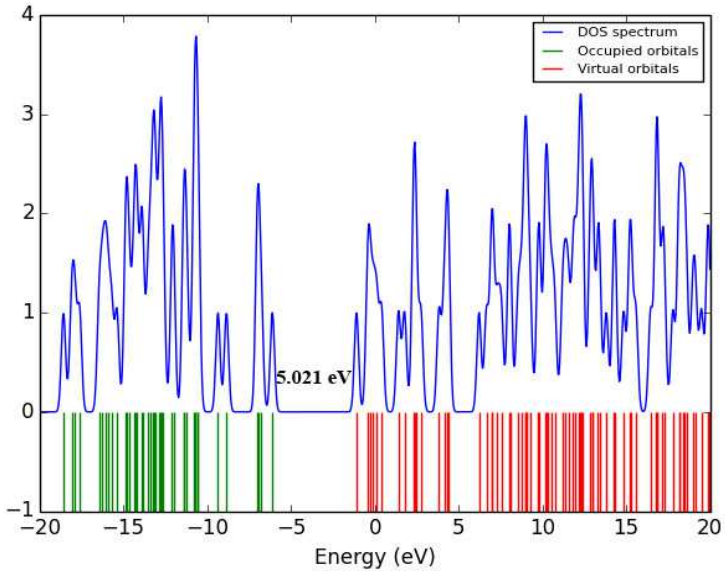

(b) B3LYP/6-311G**

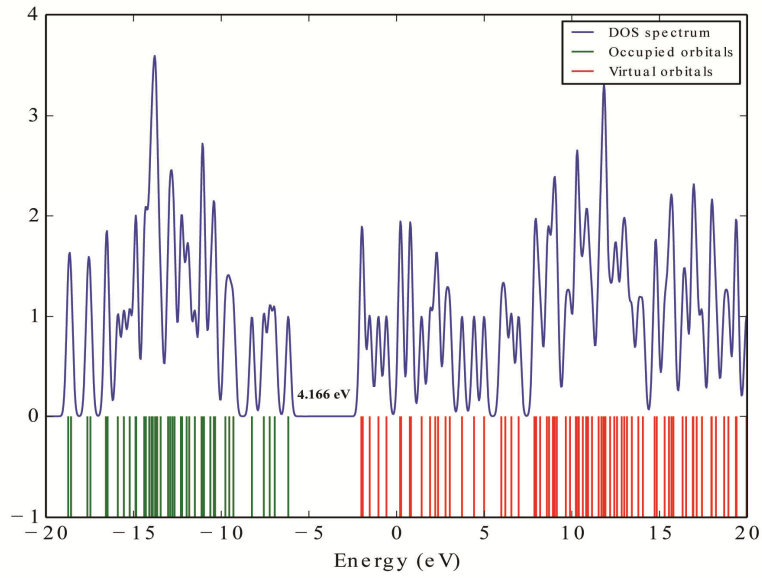

(c) TD-DFT

Figure 4: DOS of 4,4'-Diaminooctafluorobiphenyl Molecule for (a) HF/6-311G (b) B3LYP/6-311G** and (c) TD-DFT**

The calculated frontier orbital energies HOMO and LUMO and energy gaps between HOMO and LUMO are shown in Figure 4. The computed energy values of HOMO and LUMO in gas phase are 11.32 eV [HF/6-311G**]; 5.02 eV [B3LYP/6-311G**] and 4.16 eV [TD-DFT], respectively. The energy gap values are presented in Table 3. The energy gap between HOMO and LUMO determines the kinetic stability, chemical reactivity, optical polarizability, and chemical hardness-softness of a molecule. The HLG decreases from 11.32 eV to 4.16 eV. This variation is also confirmed from the spectrum of density of states (DOS) [Figure.4]. Seemingly, the significant decrease of HLG may facilitate large electron conduction and switching behaviour through the molecule.

Table 4: Frontier of Molecular Orbital Energies of 4,4'-Diaminooctafluorobiphenyl Molecule

Methods	HOMO	LUMO	Energy Gap (eV)
HF/6-311G**	-8.702	2.618	11.320
B3LYP/6-311G**	-6.112	-1.090	5.021
TD/DFT	-6.177	-2.011	4.166

One of the important applications of this work is to derive the molecular electrostatic potential (ESP) of this isolated molecule and to identify the strong electronegative and positive regions in the space of the molecule [31]. Figure 8 shows the isosurface representation of ESP, obtained from B3LYP/6-311G** level calculation. Both negative (red) and positive (blue) regions of this property are plotted at ±0.5 eÅ^{-3} isosurface values. It is clear from Figure 5 that the negative ESP is concentrated solely around the F atoms, whereas in the rest of the regions positive ESP dominates. From these results, we can say that the H atoms indicate the strongest attraction and F atom indicates the strongest repulsion. The MEP calculations have been done to predict the polarization, electron correlation and charge transfer effect within the molecule.

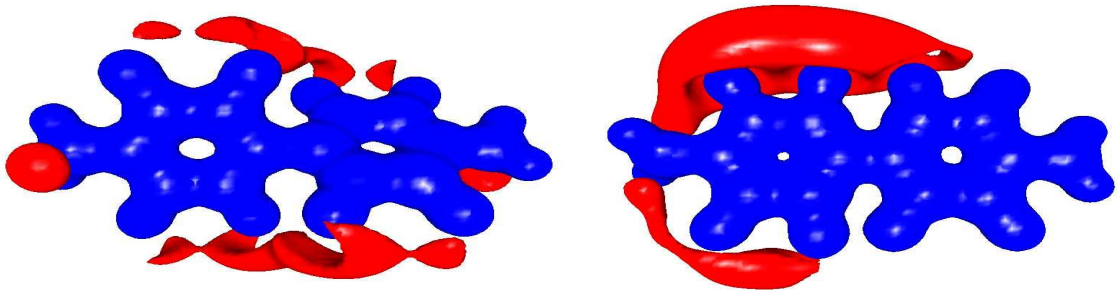

Figure 5: Isosurface Representation of ESP of 4,4'-Diaminooctafluorobiphenyl Molecule. Blue: Positive Potential (+0.5 Eå$^{-3}$), Red: Negative Potential (-0.5 Eå$^{-3}$)

VIBRATIONAL ASSIGNMENTS

Vibrational unearthly assignments of the watched groups of 44DF have been made as per the position, shape, nature and relative powers and are performed on the tentatively recorded FT-IR and FT-Raman spectra in light of the hypothetically anticipated Wave numbers by HF and DFT strategy with premise set 6-311G (d,p). 44DF has 26 particles and in this manner it has 72 ordinary methods of vibrations. Hypothetically figured frequencies of both infrared and Raman frequencies together with trial information of the 44DF atom are introduced in Table 4.

Solid trademark assimilations because of the C – X (F, Cl, Br, I) band are affected by neighbouring particles or bunches and the littler halide molecule is more impacted by the neighbouring iota. The C – F bond is the most grounded and is generally short because of its incomplete ionic character. The quality of the bond increments furthermore abbreviates as more fluorine iotas are joined to a similar carbon particle. Generally extremely exceptional C – F extending vibrations show up in the recurrence run 1360–1000 cm^{-1} [32,33]. Sun et al. [2] detailed that the trifluoroacetic corrosive shows C – F extending vibrations at 1244 and 1182 cm^{-1}. In the present review, the FT-IR groups at 1350, 1120 and 1000 cm^{-1}and the FT-Raman groups at 1111 cm^{-1} are seen as C – F extending vibrations. The registered Wave numbers of these vibrations harmonize well with the test assignments. The C-F torsion and out plane bowing of FT-IR and FT-Raman range sees at 1580 and 1578 cm^{-1}. The C–C–C bending [34-36] groups dependably happen around 600 cm^{-1} in the present work groups saw at 650 and 600 cm^{-1} in FTIR range and at 640, 580 and 430 cm^{-1} in FT Raman are relegated to C – C – C bending modes.

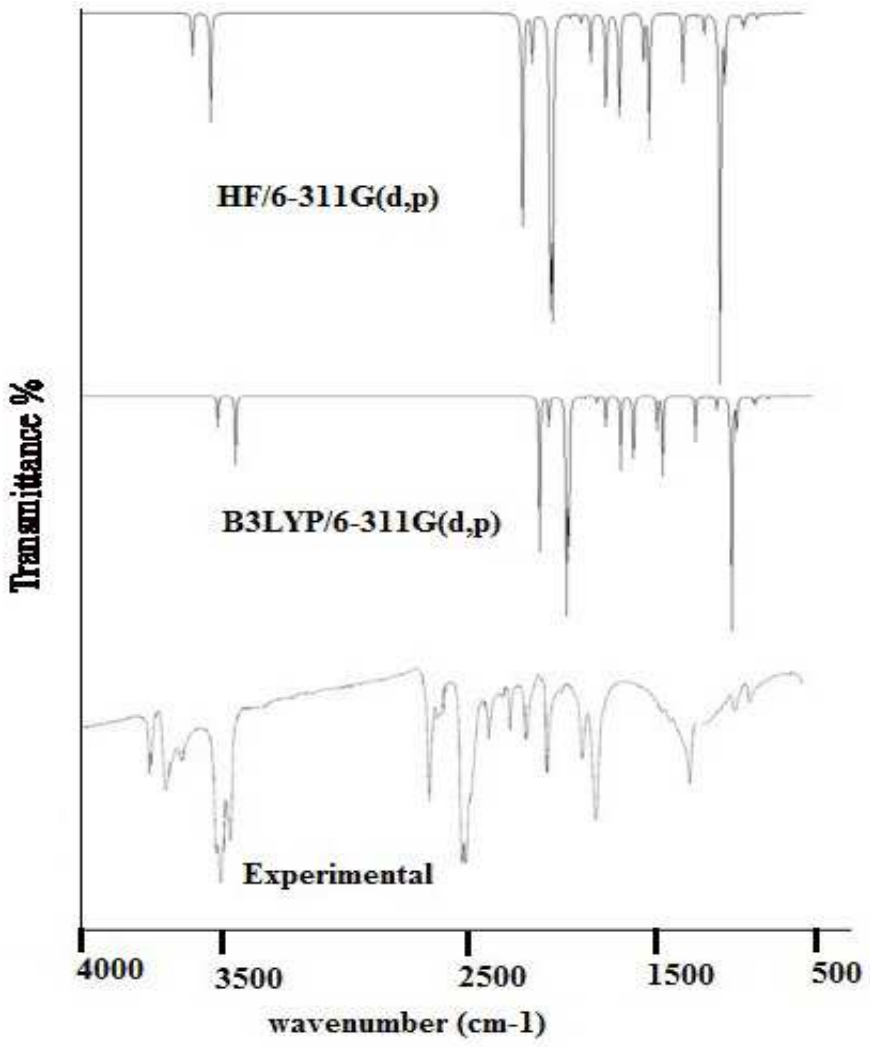

Figure 6: FT-IR Spectrum of 44DF Molecule

CONCLUSIONS

The quantum chemical calculations were performed to understand the important bonding features and transport properties of the 4,4'-Diaminooctafluorobiphenyl molecule using Bader's AIM theory. Optimized geometrical parameters of the 4,4'-Diaminooctafluorobiphenyl molecule have been calculated and compared with different methods. Importantly, the bond topological analysis indicates that aromatic Car–Car bonds are much stronger than the other bonds in the molecule. Moderate bond densities were noticed at the BCPs of the C–N and C–O bonds, but it does not lie in inter-nuclear axis. The ellipticity of ring C–C bonds are found to be small compared with other bonds in the molecule; it clearly indicates C–C bond is π-bond in nature. Further, the HOMO and LUMO orbitals have been visualized and their energy gap value is 4.40 eV. The MEP map shows that the negative potential sites are on electronegative atoms while the positive potential sites are around the hydrogen atoms: This difference may be attributed to the group charge effect. These observations give an insight on this kind of switching molecule, which are useful to design navel electronic devices.

REFERENCES

1. *Szaciłowski K, Digital information processing in molecular systems. Chemical Reviews 2008; 108(9):3481-548.*
2. *Andreasson J and Pischel U, Smart molecules at work—mimicking advanced logic operations. Chemical Society Reviews 2010; 39: 174–188.*
3. *Aviram A and Ratner M A, Molecular rectifiers. Chemical Physical Letters 1974; 29:277–283.*
4. *Reed M A, Zhou C, Muller C J, Burgin T P and Tour J M, Conductance of a Molecular Junction.Science 1997; 278: 252–254.*
5. *Balzani V, Credi A, Venturi M. 2008. Molecular Devices and Machines: Concepts and Perspectives for the Nanoworld. Weinheim: Wiley-VCH*
6. *Smit R H M, Noat Y, Untiedt C, Lang N D, van Hemert M C and van Ruitenbeek J M, Measurement of the conductance of a hydrogen molecule. Nature 2002; 419: 906–909.*
7. *Xu B and Tao N J, Measurement of single-molecule resistance by repeated formation of molecular junctions, Science 2003; 301: 1221–1223.*
8. *Morgenstern K., Switching individual molecules by light and electrons: from isomerisation to chirality flip. Progress in Surface Science 2011; 86:115–161.*
9. *Feldheim, D. L. & Keating, C. D. Self-assembly of single electron transistors and related devices, Chemical Society Reviews 1998; 27: 1–12.*
10. *Collier, C. P. A[2] catenane-based solid state electronically reconfigurable switch. Science 2000; 289: 1172–1175.*
11. *Joachim, C.; Gimzewski, J. K.; Aviram, A. Electronics using hybrid-molecular and mono-molecular devices, Nature 2000; 408: 541-548.*
12. *Kudernac T, Kobayashi T, Uyama A, Uchida K, Nakamura S, Feringa B L. Tuning the temperature dependence for switching in dithienylethene photochromic switches. Journal of Physical Chemical A 2013; 117: 8222– 8229.*
13. *Balzani V, Gomez-Lopez M, Stoddart J F. Molecular machines. Accounts in Chemical Research 1998; 31:405–14*
14. *Tian H, Wang S. Photochromic bisthienylethene as multi-function switches. Chemical Communication 2007: 781–792*
15. *Borsenberger P M, Schein L B, Hole transport in 1-phenyl-3-((diethylamino)styryl)-5-(p-(diethylamino)phenyl)pyrazoline-doped polymers, Journal of Physical Chemistry 1994; 98:233-239.*
16. *Rakhi G, Srivastava R, Rana O, Mehta D S, Kamalasanan M N, New Organic Thin-Film Encapsulation for Organic Light Emitting Diodes, Jour Encap Adsor Sci 2011; **1**:23-28.*
17. *A. Nitzan, A; Ratner, M. A. Electron transport in molecular wire junctions, Science 2003;300: 1384-1389.*
18. *deSI, Topac A, Structural features of 4, 4'-diaminooctafluorobiphenyl. Journal of Molecular Structure 2000; 526: 201–207.*
19. *Yang Y, Weaver M N, Merz Jr K M, Assessment of the "6-31+G** + LANL2DZ" Mixed Basis Set Coupled with Density Functional Theory Methods and the Effective Core Potential: Prediction of Heats of Formation and Ionization Potentials for First-Row-Transition-Metal Complexes, Journal of Physical Chemistry A 2009;**113**:9843–9851.*
20. *Frisch M J, Trucks G W, Schlegel H B, Scuseria G E, Robb M A, Cheeseman J R, Montgomery A J, Vreven T, Kudin K N, Burant J C, Millam J M, Iyengar S S, Tomasi J, Barone V, Mennucci B, Cossi M, Scalmani G, Rega N, Petersson G A, Nakatsuji H, Hada M, Ehara M, Toyota K, Fukuda R, Hasegawa J, Ishida M, Nakajima T, Honda Y, Kitao O, Nakai H, Klene M, Li X, Knox J, Hratchian H P, Cross J B, Adamo C, Jaramillo J, Gomperts R, Stratmann R E, Yazyev O, Austin A J, Cammi*

R, Pomelli C, Ochterski J W, Ayala P Y, Morokuma K, Voth G A, Salvador P, Dannenberg J J, Zakrzewski V G, Dapprich S, Daniels A D, Strain M C, Farkas O, Malick D K, Rabuck A D, Raghavachari K, Foresman J B, Ortiz J V, Cui Q, Baboul A G, Clifford S, Cioslowski J, Stefanov B B, Liu G, Liashenko A, Piskorz P, Komaromi I, Martin R L, Fox D J, Keith T, Al-Laham M A, Peng C Y, Nanayakkara A, Challacombe M, Gill P M W, Johnson B, Chen W, Wong M W, Gonzalez C, Pople J A, Gaussian 03, revision B.04. Gaussian Inc., Pittsburgh, PA, 2003

21. *Bader R F W, Nguyen-Dang T T, Quantum Theory of Atoms in Molecules–Dalton Revisited, Advance in Quantum Chemistry 1981; 14:63-124.*
22. *AIMAll (Version 10.03.25) Todd A. Keith (aim.tkgristmill.com), 2010*
23. *Perdew J P, Density-functional approximation for the correlation energy of the inhomogeneous electron gas, Physical Review B 1986;33:8822-8824.*
24. *Biegler-konig F W, Bader R F W, Tang T H, Calculation of the average properties of atoms in molecules. II, Journal of Computational Chemistry 1982; 13:317–328.*
25. *P. Srinivasan and A. David Stephen, DFT and Bader's AIM analysis of 2, 5-, diphenyl-1, 3, 4-oxadizole molecule: A organic light emitting diode (OLED), Journal of Theoretical and Computational Chemistry 2015; 14(5): 1550038-13.*
26. *Bader R F W, Atoms in Molecule: A Quantum Theory, Clarendon Press, Oxford, UK, 1990.*
27. *Cremer D, Kraka E, A description of the chemical bond in terms of local properties of electron density and energy, Croacita Chemica Acta 1984; 57(6):1259–1281.*
28. *Aihara, J, Reduced HOMO LUMO gap as an index of kinetic stability for polycyclic aromatic hydrocarbons, Journal of Physical Chemistry A 1999;103:7487–7495.*
29. *Hong S, Reifenberger R, Tian W, Datta S, Hendersonc J I, Kubiak C P, Molecular conductance spectroscopy of conjugated, phenyl-based molecules on Au(111):The effect of end groups on molecular conduction, Superlattices Microstruct 2000; 28(4):289–303.*
30. *Farmanzadeh D, Ashtiani Z, Theoretical study of a conjugated aromatic molecular wire, Structural Chemistry 2010; 21(4):691–699.*
31. *Brinck T, Murray J S, Politzer P, The electrostatic potential: An overview, International Journal of Quantum Chemistry 1992; 44(19):57–64.*
32. *G. Socrates, Infrared Characteristic Group Frequencies, Wiley Intersciences Publication, New York, 1980.*
33. *Z. H. Sun, L. Zhang, D. Xu, X. Q. Wang, X. J. Liu, G. H. Zhang, Spectrochim. Acta A 2008; 71: 663–668.*
34. *Gunasekeran S and Hemamalini R, Indian J Phys., 41 (2003) 319*
35. *Venkataraman Rao P and Ramana Rao G, Density Functional Theory and Abinitio Studies of Vibrational Spectra of Nalidixic Acid, Spectrochim Acta 2002; 3205.*
36. *Gunasekeran S, Ponnambalam U, Muthu S and Mariappan S, Vibration al spectra and normal analysis of flucytosine, Indain Journal of Pure and Applied Physics 2006; 44; 581-586.*

APPENDICES

Table 5

		B3LYP/6-311G(d,p)					HF/6-311G(d						
Species	Unscaled Frequency	Scaled Frequency	IR Intensities		RAMAN Intensities		Unscaled Frequency	Scaled Frequency	IR intensities		RAMAN Intensities		Vibrational Assignments
			Rel	Abs	Rel	Abs			Rel	Abs	Rel	Abs	
W(72)	3693	3571	41	7	70	8	3754	3412	56	9	62	11	γCCCC + τCCCC
W(71)	3692	3570	40	7	71	8	3753	3411	55	9	63	11	γCCCC + τCCCC
W(70)	3584	3466	44	8	401	46	3644	3313	47	8	308	55	γNCCC + τNCCC
W(69)	3583	3465	134	23	136	16	3644	3312	168	27	91	16	γNCCC + τNCCC
W(68)	1696	1640	401	68	4	0	1825	1659	4	1	332	59	γFCCC + τFCCC + τFCCN
W(67)	1694	1638	1	0	864	100	1824	1658	433	71	3	0	γFCCC + τFCCC
W(66)	1642	1588	4	1	62	7	1789	1626	1	0	563	100	γFCCC + τFCCC
W(65)	1641	1587	74	13	1	0	1778	1617	117	19	2	0	γFCCC + τFCCC + τFCCF
W(64)	1640	1586	1	0	0	0	1755	1596	0	0	0	0	γFCCC + τFCCC
W(63)	1631	1577	7	1	0	0	1746	1587	3	1	0	0	γFCCC + τFCCC + τFCCN
W(62)	1553	1502	0	0	111	13	1645	1495	0	0	6	1	γFCCC + τFCCC
W(61)	1535	1484	146	25	0	0	1621	1474	151	25	0	0	γFCCC + τCCCC
W(60)	1529	1478	452	77	0	0	1599	1453	563	92	0	0	τCCCC
W(59)	1516	1466	452	77	0	0	1594	1449	506	83	0	0	τCCCC
W(58)	1482	1433	0	0	291	34	1548	1407	0	0	186	33	τCCCC
W(57)	1412	1366	6	1	0	0	1469	1335	24	4	0	0	τCCCC
W(56)	1353	1308	1	0	0	0	1406	1278	0	0	6	1	τCCCC
W(55)	1345	1301	17	3	0	0	1345	1222	26	4	4	1	τCCCC
W(54)	1336	1292	0	0	38	4	1344	1222	70	11	1	0	τCCCC
W(53)	1284	1242	80	14	0	0	1344	1222	83	14	0	0	τHCNC
W(52)	1193	1153	138	24	1	0	1231	1119	0	0	0	0	τHCNC
W(51)	1193	1153	38	6	3	0	1171	1064	23	4	0	0	τHCNC
W(50)	1185	1146	0	0	1	0	1160	1054	16	3	0	0	τHCNC
W(49)	1130	1093	13	2	0	0	1155	1050	211	34	0	0	δFCC
W(48)	1119	1083	16	3	0	0	1136	1033	1	0	0	0	δFCC
W(47)	1112	1075	186	32	0	0	1123	1021	76	12	0	0	δFCC
W(46)	971	939	0	0	40	5	1016	923	0	0	14	2	δFCC
W(45)	966	934	87	15	0	0	1014	921	139	23	0	0	δFCC
W(44)	932	902	206	35	0	0	978	889	290	47	0	0	δFCC
W(43)	781	755	0	0	0	0	858	780	0	0	2	0	δFCC
W(42)	765	740	0	0	1	0	852	774	0	0	0	0	δFCC
W(41)	729	705	108	18	1	0	804	731	15	3	0	0	δCCC
W(40)	702	678	0	0	0	0	795	723	0	0	0	0	δNCC
W(39)	686	663	3	1	0	0	765	695	205	34	1	0	δNCC
W(38)	663	641	2	0	0	0	755	686	8	1	3	0	δCCC
W(37)	649	627	0	0	19	2	753	684	2	0	4	1	δCCC
W(36)	646	624	0	0	0	0	750	681	0	0	0	0	δCCC
W(35)	643	621	5	1	0	0	736	669	21	3	1	0	δCCC
W(34)	603	583	3	0	36	4	693	630	65	11	28	5	δCCC
W(33)	597	578	32	5	2	0	684	621	612	100	1	0	δCCC
W(32)	518	500	36	6	17	2	611	555	9	1	14	2	δCCC
W(31)	504	488	585	100	2	0	605	550	76	12	3	0	δHNH + δHNC
W(30)	498	481	30	5	20	2	559	508	22	4	1	0	δHCN
W(29)	474	458	102	17	3	0	558	507	10	2	1	0	δHNH + δHNC
W(28)	456	441	0	0	2	0	526	478	1	0	28	5	δHCN
W(27)	449	434	0	0	7	1	502	456	13	2	3	1	δCCC + ϑCC
W(26)	413	400	1	0	1	0	498	453	0	0	0	0	δCCC + ϑCC
W(25)	413	399	3	0	23	3	491	447	1	0	10	2	ϑFC
W(24)	401	387	3	1	3	0	491	446	0	0	2	0	ϑFC
W(23)	372	360	13	2	0	0	476	433	0	0	7	1	ϑFC
W(22)	371	359	0	0	2	0	469	426	1	0	6	1	ϑFC
W(21)	359	347	14	2	6	1	441	401	3	0	1	0	ϑFC
W(20)	358	346	8	1	3	0	402	366	0	0	1	0	ϑFC
W(19)	342	330	7	1	0	0	377	343	12	2	0	0	ϑFC
W(18)	306	296	0	0	0	0	343	312	0	0	0	0	ϑFC
W(17)	304	294	0	0	0	0	342	311	0	0	0	0	ϑCC
W(16)	288	278	0	0	1	0	326	297	3	0	0	0	ϑNC
W(15)	283	273	0	0	0	0	326	296	6	1	0	0	ϑNC
W(14)	279	270	2	0	1	0	324	294	0	0	1	0	ϑCC
W(13)	279	270	7	1	0	0	321	291	0	0	0	0	ϑCC

W(12)	233	225	3	1	0	0	304	276	1	0	0	0	ϑCC
W(11)	229	221	0	0	0	0	301	273	3	0	0	0	ϑCC
W(10)	185	179	0	0	2	0	217	197	1	0	0	0	ϑCC
W(9)	183	177	0	0	1	0	212	193	1	0	0	0	ϑCC
W(8)	180	174	2	0	0	0	201	182	0	0	2	0	ϑCC
W(7)	142	137	2	0	0	0	180	164	0	0	1	0	ϑCC
W(6)	142	137	0	0	2	0	173	157	2	0	0	0	ϑCC
W(5)	133	128	0	0	0	0	172	156	0	0	0	0	ϑCC
W(4)	130	126	0	0	1	0	158	143	0	0	1	0	ϑNH
W(3)	52	50	1	0	2	0	89	81	1	0	2	0	ϑNH
W(2)	42	41	2	0	2	0	82	75	1	0	1	0	ϑNH
W(1)	37	35	0	0	5	1	81	73	0	0	3	0	ϑNH

ϑ – Stretching
δ – Bending
τ – Torsion
γ – Out of plane bending